ACS APPLIED MATERIALS & INTERFACES

Research Article

www.acsami.org

Millisecond Laser Ablation of Molybdenum Target in Reactive Gas toward MoS_2 Fullerene-Like Nanoparticles with Thermally Stable Photoresponse

Shu-Tao Song, Lan Cui, Jing Yang,* and Xi-Wen Du*

Institute of New-Energy Materials, School of Materials Science and Engineering, Tianjin University, Tianjin 300072, People's Republic of China

Supporting Information

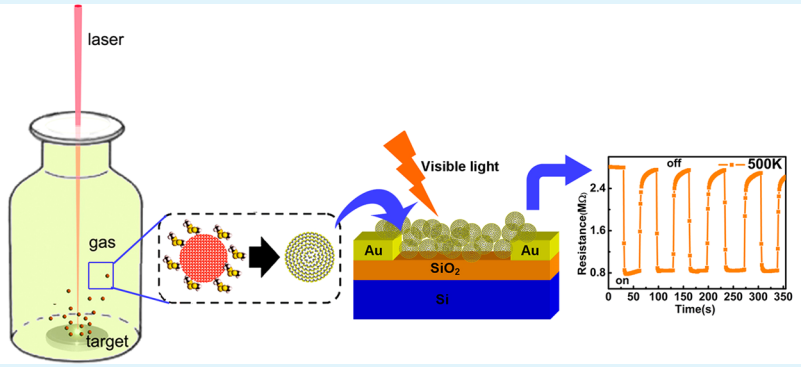

ABSTRACT: As a promising material for photoelectrical application, MoS_2 has attracted extensive attention on its facile synthesis and unique properties. Herein, we explored a novel strategy of laser ablation to synthesize MoS_2 fullerene-like nanoparticles (FL-NPs) with stable photoresponse under high temperature. Specifically, we employed a millisecond pulsed laser to ablate the molybdenum target in dimethyl trisulfide gas, and as a result, the molybdenum nanodroplets were ejected from the target and interacted with the highly reactive ambient gas to produce MoS_2 FL-NPs. In contrast, the laser ablation in liquid could only produce core−shell nanoparticles. The crucial factors for controlling final nanostructures were found to be laser intensity, cooling rate, and gas reactivity. Finally, the MoS_2 FL-NPs were assembled into a simple photoresponse device which exhibited excellent thermal stability, indicating their great potentialities for high-temperature photoelectrical applications.

KEYWORDS: *laser ablation, MoS_2 nanoparticles, photoresponse*

1. INTRODUCTION

Molybdenum disulfide (MoS_2) possesses a direct band gap of 1.8 eV (for monolayer structure) and an indirect band gap of 1.2 eV (for bulk material),[1−5] which are efficient for the absorption of sun light. Hitherto, MoS_2 materials have been widely applied in photocatalytic hydrogen evolution,[6−9] lithium ion batteries,[10] field effect transistors,[1,3] and so on. Besides the common planar layer structure, MoS_2 material can be manufactured into fullerene-like nanoparticles (FL-NPs) under appropriate conditions as well,[11−13] and such a structure exhibits many unique properties, especially superior tribological behavior under high loads.[12,14]

Hitherto, MoS_2 FL-NPs have been successfully fabricated via several high-temperature processes such as thermal evaporation and catalyzed transport.[15,16] However, these processes are usually time and energy consuming, thus it is still a big challenge to find a rapid and efficient way to produce MoS_2 FL-NPs. One possible solution is to adopt laser ablation (LA) technique which is well-known for its simplicity, rapidity, and low-temperature sythesis.[17−19] To date, much attention has been paid to laser ablation in liquid (LAL), where a solid target is ablated to generate primary products in gas or plasma state, which then react with the liquid medium to produce the final compound nanoparticles.[20−23] However, this method meets tremendous difficulties when refractory metals are adopted as targets for the preparation of sulfides. First, the primary phase is often quenched due to the endothermic vaporization and high thermal conductivity of the liquid medium,[20,24] and the quenching effect for the refractory metals becomes more pronounced than that for low melting metals, which impedes subsequent reactions.[25] Moreover, the reaction of laser generated plasma with liquid medium is relatively uncontrollable[22] and usually causes byproducts such as carbides or oxides.[26,27] As a result, refractory-metal-sulfide nanostructures have never been produced by laser ablation of metal targets in liquid medium so far.

Received: November 5, 2014
Accepted: January 8, 2015
Published: January 8, 2015

DOI: 10.1021/am508750y
ACS Appl. Mater. Interfaces 2015, 7, 1949−1954

Compared with liquid medium, gaseous environments can provide a slower cooling rate for complete reaction. Therefore, we propose that laser ablation in gas (LAG) may open up a new avenue toward fabrication of sulfides nanostructures from refractory metal targets. Moreover, the utilization of MoS_2 FL-NPs are rather limited and mainly concentrated on tribology and polymer reinforcement.[12,28,29] Considering that MoS_2 owns an ideal band gap for efficient light absorption and the closed surface of the MoS_2 FL-NPs provides a kinetic hindrance against oxidation in air,[30] we conceive that the MoS_2 FL-NPs can serve as a photoresponse material for optoelectronic device with excellent thermal resistance.

In the present work, we employ a long-pulse-width (millisecond) laser with lower power density (10^6–10^7 W/cm^2) to ablate the molybdenum target in dimethyl trisulfide (DMTS, CH_3-S-S-S-CH_3). The LAG process first generate a large amount of hot molybdenum nanodroplets, which then react with ambient DMTS to produce MoS_2 FL-NPs.[22,31−33] The MoS_2 FL-NPs exhibit excellent photoresponse performance at high temperature. To the best of our knowledge, this is the first report on the synthesis of MoS_2 FL-NPs by LAG and their photoelectrical applications, and our approach embodies many unique advantages, such as simplicity, facility, and rapidity.

2. EXPERIMENTAL SECTION

LAG Synthesis. The experimental setup was schematically illustrated in Supporting Information, Scheme S1. A piece of Mo target (5 mm thick, purity quotient 99.99%) was ablated by using a millisecond pulsed Nd:YAG laser (wavelength 1064 nm) in DMTS gas which was carried into the reactor by argon gas (99.99%, Kunteng Gas, Tianjin, China) with a flow rate of 60 sccm. The single-pulse energy, pulse width, and frequency used in the experiments were 45 (or 25) J/pulse, 20 ms, and 1 Hz, respectively, and the laser ablation was kept for 15 min. The products were deposited on a substrate or dispersed in a solvent for further characterization. The product yield of MoS_2 FL-NPs was measured as 3 mg/h. For the preparation of pure Mo NPs, pure argon gas was adopted as the protective gas with a flow rate of 60 sccm, and the other parameters and processes were kept constant.

LAL Synthesis. The experimental setup was schematically illustrated in Supporting Information, Scheme S2. The Mo target (5 mm thick, purity quotient 99.99%) was immersed in 12 mL of DMTS with a solution depth of 5 mm above the target surface and ablated by the millisecond pulsed Nd:YAG laser. The synthetic system was protected by Ar gas at a flow rate of 60 sccm. The single-pulse energy, pulse width, and frequency used in the experiments were 45 J/pulse, 20 ms, and 1 Hz, respectively, and the irradiation was kept for 15 min. After the laser ablation, the suspension was centrifuged at 12000 rpm, washed with ethanol for three times, and finally dispersed in ethanol.

Photoresponse Measurement. Photoresponse devices were fabricated by depositing the NPs prepared via the LAG process directly on the oxidized silicon substrate with Au interdigital electrodes, as shown in Supporting Information, Scheme S1. The NPs by LAL were first concentrated by centrifugalization and then coated on the oxidized silicon substrate with Au interdigital electrodes. The MoS_2 FL-NPs sample was annealed at 300 °C for 2 h so as to stabilize the structure. The performance of the devices was measured both in the dark and under AM 1.5G white light irradiation in a simulated sunlight illumination system (100 mW/cm^2, Sciencetech, SS150).

Characterization. The product morphology was observed by using a Hitachi S-4800 scanning electron microscope (SEM) and FEI Technai G2 F20 transmission electron microscope (TEM) equipped with a field-emission gun, and the composition was measured by an Oxford INCA energy dispersive spectroscopy (EDS) and Gatan Tridiem 863 electron energy loss spectroscopy (EELS) module attached to the TEM. The phase structure was investigated by using a Bruker D8 advance X-ray diffraction (XRD). UV−vis absorption spectra were detected by using a Hitachi U4100 spectrophotometer. Raman spectra were detected by using a Thermo Fisher Scientific DXR Microscope. Fourier transformed infrared (FTIR) spectra were recorded using a Bruker Tensor 27 spectrometer.

3. RESULTS AND DISCUSSION

First, we compare the product obtained in pure argon and that in the mixed gas of DMTS and argon. As shown in the top inset of Figure 1a, the main product in pure argon is composed of

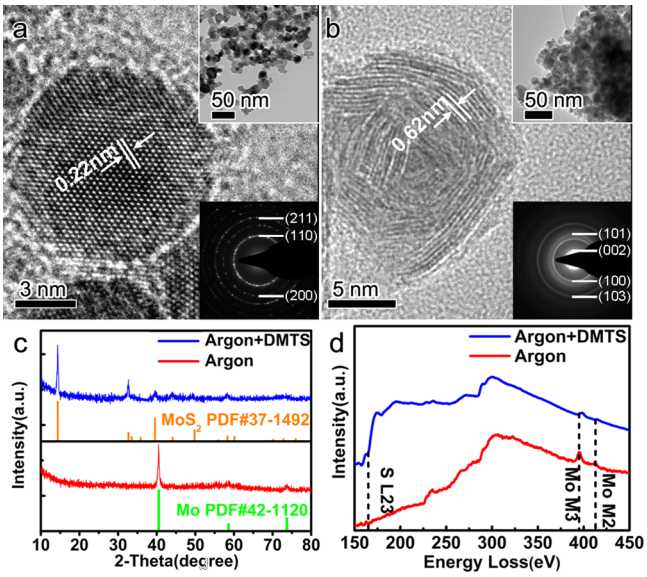

Figure 1. Characterizations of nanoparticles prepared by LAG in different ambient gas. (a) HRTEM image of Mo NPs obtained in pure argon. Insets: TEM image (top) and SAED pattern (bottom) of Mo NPs, respectively. (b) HRTEM image of MoS_2 FL-NPs obtained in the mixed gas of argon and DMTS. Insets: TEM image (top) and SAED pattern (bottom) of MoS_2 NPs, respectively. (c) XRD patterns and (d) EELS spectra after background subtraction and plural scattering removal.

fine nanoparticles with an average size around 20 nm, and the high-resolution TEM (HRTEM) image shows clear lattice fringes with a spacing of 0.22 nm, corresponding to the (110) plane of body-centered-cubic structure of bulk molybdenum. Other characterizations, such as selected area electronic diffraction (SAED, see the bottom inset of Figure 1a), XRD (Figure 1c), and EELS (Figure 1d) collectively indicate that the nanoparticles consist of pure molybdenum.[34]

After the molybdenum target was ablated with high single-pulse energy (45 J/pulse) in the mixed gas of Ar and DMTS, a large amount of FL-NPs were obtained in the product (Figure 1b and its top inset). XRD profile (Figure 1c) and SAED (the bottom inset of Figure 1b) jointly illustrate that the NPs are composed of hexagonal 2H-MoS_2 (PDF no. 37-1492), and no impurity is detected. The HRTEM image of MoS_2 nanoparticle reveals a nested nature, and the (002) planes of hexagonal MoS_2 are clearly observed (Figure 1b). EDS analysis suggests that the NPs only contain molybdenum and sulfur elements, and the sulfur to molybdenum ratio is close to 2:1 (Supporting Information, Figure S1b). EELS spectrum (blue line in Figure 1d) exhibits weak S-edge and Mo-M lines, the Mo peaks shift positively from the position of pure molybdenum, and the S-edge at 162.5 eV shifts negatively from that of element sulfur (165 eV), being consistent with the presence of S^{2-} ions.[34]

DOI: 10.1021/am508750y
ACS Appl. Mater. Interfaces 2015, 7, 1949−1954

Raman spectrum of the FL-NPs shows typical MoS_2 bands at 408 and 384 cm^{-1}, corresponding to A_{1g} and E_{2g}^1 vibrations, respectively (Supporting Information, Figure S1c).[35] FTIR spectrum reveals Mo−S stretching vibration at 467 cm^{-1} (Supporting Information, Figure S1d).[36] All the above results confirm that MoS_2 FL-NPs can be produced by pulsed laser ablation of molybdenum target in reactive gas at room temperature.

When the laser pulse energy decreases to 25 J/pulse, the main product is composed of core−shell NPs with sizes around 30 nm, as indicated in Figure 2a and Supporting Information,

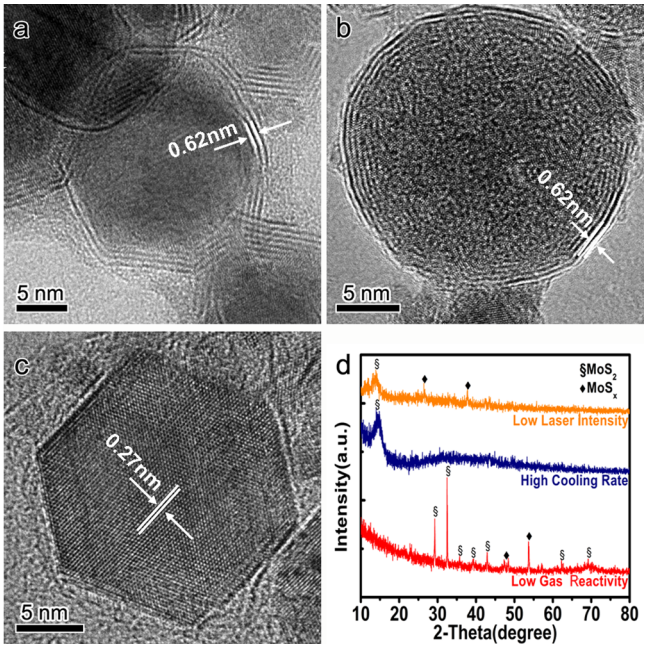

Figure 2. Products obtained under various experimental conditions. (a) HRTEM image of NPs obtained at lower laser intensity. (b) HRTEM image of NPs obtained at high cooling rate in liquid DMTS. (c) HRTEM image of NPs obtained in DMS with low reactivity. (d) XRD patterns of the above three samples.

Figure S2a1. The shell exhibits obvious inorganic fullerene-like structure with interplanar distances of 0.62 nm corresponding to (002) planes of MoS_2, while the core shows low crystallinity in the HRTEM image (Figure 2a). XRD result indicates that the product comprises of two phases, namely MoS_2 (PDF no. 37-1492) and nonstoichiometric molybdenum subsulfide (MoS_x) (Figure 2d, orange line). The above results jointly illustrate that the product is composed of MoS_x @ MoS_2 core−shell nanoparticles.

We then compare the LAG with the LAL technique by performing laser ablation in liquid DMTS with the same parameters as in LAG. As can be seen in Supporting Information, Figure S2b1, the product consists of nanoparticle with the sizes of 10−30 nm. The HRTEM image (Figure 2b) depicts a core−shell structure. The shell exhibits a layered structure with interplanar distances of 0.62 nm, which agrees with the (002) lattice fringe of MoS_2, while the core presents an amorphous structure. The SAED pattern shows a blur feature with weak (002) ring of MoS_2 (Supporting Information, Figure S2b2), and XRD profile exhibits an intensive MoS_2 (002) peak (blue line in Figure 2d). Furthermore, EDS line-scan analysis indicates that the NPs are composed of Mo and S elements (Supporting Information, Figure S3). On the basis of the above, we can conclude that the products by LAL consist of amorphous MoS_x NPs coated with a thin MoS_2 shell.

When DMTS was replaced with a less reactive sulfur source, dimethyl sulfide (DMS, CH_3-S-CH_3),[37] the product is found to comprise of hexagonal nanoplates (Figure 2c and Supporting Information, Figure S2c1), which have been found in other works.[38−40] The HRTEM image shows lattice fringe with a spacing of 0.27 nm, corresponding to (103) planes of 2H-MoS_2 (Figure 2c). The XRD (red line Figure 2d) and SAED (Supporting Information, Figure S2c2) patterns suggest the formation MoS_2 and MoS_x, which implies that the sulfidation reaction in DMS is not sufficient.

On the basis of the above, we propose a possible mechanism for the growth of MoS_2 nanostructures by LAG. Millisecond laser could only heat the target into a partially molten state due to its lower power density (10^6−10^7 W/cm^2), and the primary products ejected from the target comprise mainly metal nanodroplets (Scheme 1a).[22,31−33] Subsequently, the metal

Scheme 1. Schematic Illustration for the Formation of MoS_2 Nanostructures[a]

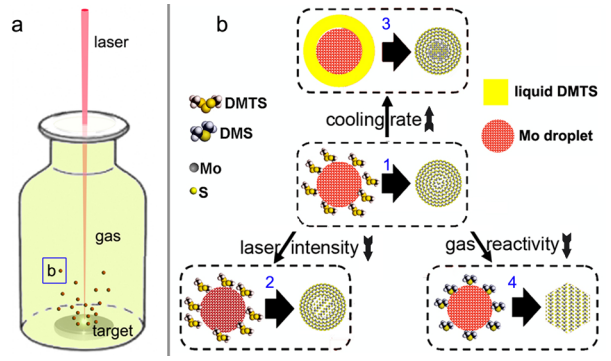

[a](a) The formation of molybdenum nanodroplets in LAG; (b) the effect of laser intensity, cooling rate, and sulfur source reactivity on the morphology of nanostructures in Mo/S system.

nanodroplets react with the ambient medium by surface reactions, which proceed layer by layer from the surface to interior before the cooling of the nanodroplets[31−33] and gives rise to different nanostructures depending on the cooling rate, laser intensity, and gas reactivity (Scheme 1b). For the synthesis of MoS_2 FL-NPs, the definitive factor is to maintain the high temperature of metal nanodroplets.[41] As shown in Scheme 1b, pure MoS_2 FL-NPs could be produced only at low cooling rate, high laser intensity, and high gas reactivity, where the molybdenum nanodroplets retains at high temperature for a long period which promotes the diffusion of sulfur atoms and guarantees a complete surface reaction (route 1). When the laser intensity descends, the ceiling temperature of metal nanodroplets decreases,[42−44] leading to an incomplete surface reaction and MoS_x−MoS_2 core−shell nanoparticles (route 2). When the laser ablation is conducted in liquid DMTS, the cooling rate of molybdenum nanodroplets is remarkably accelerated due to the vaporization and high thermal conductivity of the liquid, therefore the surface reaction of molybdenum nanodroplets is quenched, resulting in a core−shell structure with an amorphous core and a MoS_2 shell (route 3). Moreover, the sulfidation potential of reactive gas also shows a significant effect on the surface reaction rate. When DMS is adopted as the reactive gas, its low sulfidation potential

DOI: 10.1021/am508750y
ACS Appl. Mater. Interfaces 2015, 7, 1949−1954

causes a nanoplate-like MoS_2 nanostructure instead of FL-NPs (route 4). The formation of nanoplates is not well understood yet and needs further investigation.

Next, we detected the light absorption capability of FL-NPs. As shown in Supporting Information, Figure S4 (blue line), the absorption spectrum presents typical absorption peaks between 600 and 700 nm arising from the direct band transition, while the broad absorption tail longer than 700 nm corresponds to the indirect band transition.[45] Considering its superior absorption properties, we then assembled the FL-NPs into a photodetector by depositing the FL-NPs on an insulating substrate with gold electrode (see Figure 3a). The measurements were performed at temperatures ranging from 300 to 500 K. As shown in Figure 3b–d, the electrical resistance of the device drops down dramatically when exposed under the incident light. Meanwhile, the response and recovery rates increase significantly with the increasing temperatures, the response time reduces from 92 s at 300 K to 2 s at 400 K and then 1.4 s at 500 K, while the recovery time varies from 64 s at 300 K to 41 s at 400 K and then 3 s at 500 K. As well, the sensitivity of the device increases with the working temperature (see Table 1). As summarized in Table 2, the device constructed MoS_2 FL-NPs presents higher response rate than other devices reported in literature. In contrast, the devices constructed by other NPs show rather weak photoresponse at 300 K (see Supporting Information, Figure S5).

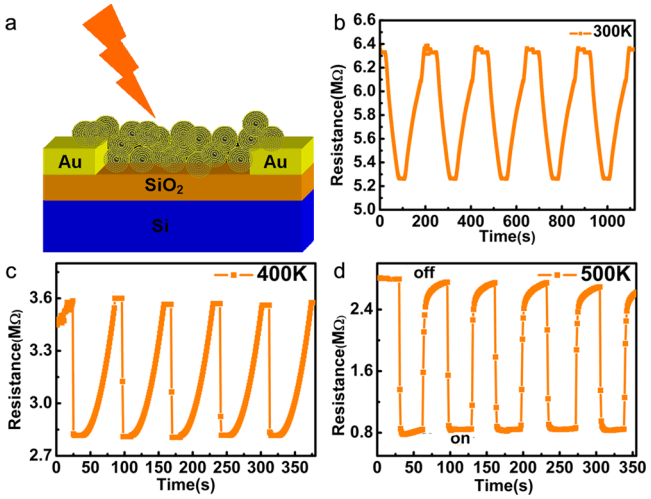

Figure 3. Photoresponse characteristics of the MoS_2 FL-NPs deposited on the Au interdigital electrode sputtered on the oxidized silicon substrate at different temperature. (a) Schematic diagram of the device for photoresponse. (b–d) Photoresponse behaviors with on–off cycles at 300, 400, and 500 K, respectively.

Table 1. Photoresponse Data of MoS_2 FL-NPs at 300, 400, and 500 K, Respectively

temperature (K)	response time (s)	recovery time (s)	resistance (M Ω)	sensitivity
300	92	64	6.3	1.14
400	2	41	3.6	1.26
500	1.4	3	2.8	3.5

Table 2. Performance Summary of MoS_2 Photodetectors

structure	response time	recovery time	ref
thin film	a few s	a few s	49
monolayer	4 s	9 s	50
nanosheets	50 ms	50 ms	51
FL-NPs	1.4 s	3 s	this work

Such an excellent high-temperature performance can be understood from two aspects: first, the high temperature improves the connection of MoS_2 FL-NPs and eliminates the defects, and as a result, the combination of electrons and holes is depressed to a large extent and more photogenerated carriers can contribute to the optoelectronic response.[46] In contrast, the device without the annealing treatment at 573 K shows very weak photoresponse (see Supporting Information, Figure S6). Second, for the highly resistive MoS_2 FL-NPs, the thermal activation helps the electron transition and improves the conductivity, thus magnifying the photocurrent and reducing the response and recovery time.[47,48]

4. CONCLUSION

We demonstrate that millisecond pulsed laser ablation of molybdenum target in reactive gas is a facile and rapid strategy for the fabrication of MoS_2 FL-NPs. The crucial factors for controlling final nanostructures include laser intensity, cooling rate, and gas reactivity. The MoS_2 FL-NPs show excellent photoresponse property at high temperatures. We believe that this strategy can be expanded to other material systems for the synthesis of various refractory-metal-sulfide nanostructures. Moreover, the stable photoresponse under high temperatures demonstrate the feasibility of using MoS_2 FL-NPs for heat-resistant photodetectors and photoelectric switches.

■ ASSOCIATED CONTENT

Ⓢ Supporting Information

Schematic diagram of the setup for the LAG and LAL processes, SEM image, EDS spectrum, FTIR spectrum,and Raman spectrum of MoS_2 FL-NPs, TEM images, and SAED patterns of the NPs obtained by varying experimental conditions. EDS line scan profile of the LAL products, absorption spectra of nanoparticles with different laser intensity, photoresponse of the NPs obtained by varying experimental conditions, photoresponse of unannealed MoS_2 FL-NPs at 300 K. This material is available free of charge via the Internet at http://pubs.acs.org.

■ AUTHOR INFORMATION

Corresponding Authors

*For X.-W.D: E-mail: xwdu@tju.edu.cn.
*For J.Y.: E-mail: yang_jing@tju.edu.cn.

Notes

The authors declare no competing financial interest.

■ ACKNOWLEDGMENTS

This work was supported by the National Basic Research Program of China (2014CB931703) and the Natural Science Foundation of China (nos. 51471115 and 51171127).

■ REFERENCES

(1) Liu, K. K.; Zhang, W.; Lee, Y. H.; Lin, Y. C.; Chang, M. T.; Su, C. Y.; Chang, C. S.; Li, H.; Shi, Y.; Zhang, H.; Lai, C. S.; Li, L. J. Growth of Large-Area and Highly Crystalline MoS_2 Thin Layers on Insulating Substrates. *Nano Lett.* **2012**, *12*, 1538–1544.

(2) Kong, D.; Wang, H.; Cha, J. J.; Pasta, M.; Koski, K. J.; Yao, J.; Cui, Y. Synthesis of MoS_2 and $MoSe_2$ Films with Vertically Aligned Layers. *Nano Lett.* **2013**, *13*, 1341–1347.

DOI: 10.1021/am508750y
ACS Appl. Mater. Interfaces 2015, 7, 1949–1954

(3) Wang, X.; Feng, H.; Wu, Y.; Jiao, L. Controlled Synthesis of Highly Crystalline MoS_2 Flakes by Chemical Vapor Deposition. *J. Am. Chem. Soc.* **2013**, *135*, 5304−5307.
(4) Radisavljevic, B.; Radenovic, A.; Brivio, J.; Giacometti, V.; Kis, A. Single-Layer MoS_2 Transistors. *Nature Nanotechnol.* **2011**, *6*, 147−150.
(5) Kuc, A.; Zibouche, N.; Heine, T. Influence of Quantum Confinement on the Electronic Structure of the Transition Metal Sulfide TS_2. *Phys. Rev. B* **2011**, *83*, 245213.
(6) Zong, X.; Yan, H.; Wu, G.; Ma, G.; Wen, F.; Wang, L.; Li, C. Enhancement of Photocatalytic H_2 Evolution on CdS by Loading MoS_2 as Cocatalyst under Visible Light Irradiation. *J. Am. Chem. Soc.* **2008**, *130*, 7176−7177.
(7) Hou, Y.; Laursen, A. B.; Zhang, J.; Zhang, G.; Zhu, Y.; Wang, X.; Dahl, S.; Chorkendorff, I. Layered Nanojunctions for Hydrogen-Evolution Catalysis. *Angew. Chem., Int. Ed.* **2013**, *52*, 3621−3625.
(8) Nguyen, M.; Tran, P. D.; Pramana, S. S.; Lee, R. L.; Batabyal, S. K.; Mathews, N.; Wong, L. H.; Graetzel, M. In Situ Photo-Assisted Deposition of MoS_2 Electrocatalyst onto Zinc Cadmium Sulphide Nanoparticle Surfaces to Construct an Efficient Photocatalyst for Hydrogen Generation. *Nanoscale* **2013**, *5*, 1479.
(9) Tang, M. L.; Grauer, D. C.; Lassalle-Kaiser, B.; Yachandra, V. K.; Amirav, L.; Long, J. R.; Yano, J.; Alivisatos, A. P. Structural and Electronic Study of an Amorphous MoS_3 Hydrogen-Generation Catalyst on a Quantum-Controlled Photosensitizer. *Angew. Chem., Int. Ed.* **2011**, *50*, 10203−10207.
(10) Stephenson, T.; Li, Z.; Olsen, B.; Mitlin, D. Lithium Ion Battery Applications of Molybdenum Disulfide (MoS_2) Nanocomposites. *Energy Environ. Sci.* **2014**, *7*, 209.
(11) Tenne, R. Inorganic Nanotubes and Fullerene-Like Materials. *Chemistry* **2002**, *8*, 5296−5304.
(12) Tenne, R. Inorganic Nanotubes and Fullerene-Like Nanoparticles. *Nature Nanotechnol.* **2006**, *1*, 103−111.
(13) Margulis, L.; Salltra, G.; Tenne, R. Nested Fullerene-Like Structures. *Nature* **1993**, *365*, 113−114.
(14) Rapoport, L.; Fleischer, N.; Tenne, R. Applications of WS_2(MoS_2) Inorganic Nanotubes and Fullerene-Like Nanoparticles for Solid Lubrication and for Structural Nanocomposites. *J. Mater. Chem.* **2005**, *15*, 1782−1788.
(15) Tenne, R.; Homyonfer, M.; Feldman, Y. Nanoparticles of Layered Compounds with Hollow Cage Structures (Inorganic Fullerene-Like Structures). *Chem. Mater.* **1998**, *10*, 3225−3238.
(16) Zak, A.; Feldman, Y.; Alperovich, V.; Rosentsveig, R.; Tenne, R. Growth Mechanism of MoS_2 Fullerene-Like Nanoparticles by Gas-Phase Synthesis. *J. Am. Chem. Soc.* **2000**, *122*, 11108−11116.
(17) Parilla, P. A.; Dillon, A. C.; Jones, K. M.; Riker, G.; Schulz, D. L.; Ginley, D. S.; Heben, M. J. The First True Inorganic Fullerenes? *Nature* **1999**, *397*, 114−114.
(18) Compagnini, G.; Sinatra, M. G.; Messina, G. C.; Patanè, G.; Scalese, S.; Puglisi, O. Monitoring the Formation of Inorganic Fullerene-Like MoS_2 Nanostructures by Laser Ablation in Liquid Environments. *Appl. Surf. Sci.* **2012**, *258*, 5672−5676.
(19) Wu, H.; Yang, R.; Song, B.; Han, Q.; Li, J.; Zhang, Y.; Fang, Y.; Tenne, R.; Wang, C. Biocompatible Inorganic Fullerene-Like Molybdenum Disulfide Nanoparticles Produced by Pulsed Laser Ablation in Water. *ACS Nano* **2011**, *5*, 1276−1281.
(20) Zeng, H.; Du, X. W.; Singh, S. C.; Kulinich, S. A.; Yang, S.; He, J.; Cai, W. Nanomaterials via Laser Ablation/Irradiation in Liquid: A Review. *Adv. Funct. Mater.* **2012**, *22*, 1333−1353.
(21) Yang, J.; Ling, T.; Wu, W. T.; Liu, H.; Gao, M. R.; Ling, C.; Li, L.; Du, X. W. A Top−Down Strategy towards Monodisperse Colloidal Lead Sulphide Quantum Dots. *Nature Commun.* **2013**, *4*, 1695−1670.
(22) Niu, K. Y.; Yang, J.; Kulinich, S. A.; Sun, J.; Li, H.; Du, X. W. Morphology Control of Nanostructures via Surface Reaction of Metal Nanodroplets. *J. Am. Chem. Soc.* **2010**, *132*, 9814−9819.
(23) Amendola, V.; Meneghetti, M. What Controls the Composition and the Structure of Nanomaterials Generated by Laser Ablation in Liquid Solution? *Phys. Chem. Chem. Phys.* **2013**, *15*, 3027.
(24) McLaughlin, E. The Thermal Conductivity of Liquids and Dense Gases. *Chem. Rev.* **1964**, *64*, 389−428.
(25) Sundstrom, D. W.; DeMichiell, R. L. Quenching Processes for High Temperature Chemical Reactions. *Ind. Eng. Chem. Process Des. Dev.* **1971**, *10*, 114−122.
(26) Franzel, L.; Phumisithikul, K.; Bertino, M. F.; Carpenter, E. E. Synthesis of Multiphasic Inhomogeneous Mo/MoC Nanoparticles by Pulsed Laser Ablation. *J. Nanopart. Res.* **2013**, *15*, 2032−2037.
(27) Liu, P.; Liang, Y.; Lin, X.; Wang, C.; Yang, G. A General Strategy to Fabricate Simple Polyoxometalate Nanostructures: Electrochemistry-Assisted Laser Ablation in Liquid. *ACS Nano* **2011**, *5*, 4748−4755.
(28) Naffakh, M.; Martin, Z.; Fanegas, N.; Marco, C.; Gomez, M.; Jiménez, I. Influence of Inorganic Fullerene-Like WS_2 Nanoparticles on the Thermal Behavior of Isotactic Polypropylene. *J. Polym. Sci., Part B: Polym. Phys.* **2007**, *45*, 2309−2321.
(29) Naffakh, M.; Marco, C.; Gómez-Fatou, M. A. Isothermal Crystallization Kinetics of Novel Isotactic Polypropylene/MoS_2 Inorganic Nanotube Nanocomposites. *J. Phys. Chem. B* **2011**, *115*, 2248−2255.
(30) Schuffenhauer, C.; Wildermuth, G.; Felsche, J. R.; Tenne, R. How Stable are Inorganic Fullerene-Like Particles? Thermal Analysis (STA) of Inorganic Fullerene-Like NbS_2, MoS_2, and WS_2 in Oxidizing and Inert Atmospheres in Comparison with the Bulk Material. *Phys. Chem. Chem. Phys.* **2004**, *6*, 3991−4002.
(31) Lv, K. M.; Yang, J.; Niu, K. Y.; Wang, H. L.; Sun, J.; Du, X. W. Synthesis of Si-C Nanostructures by Laser Ablation of Silicon Target in *N*-Heptane Vapor. *Mater. Lett.* **2009**, *63*, 2492−2494.
(32) Lin, F.; Yang, J.; Lu, S. H.; Niu, K. Y.; Liu, Y.; Sun, J.; Du, X. W. Laser Synthesis of Gold/Oxide Nanocomposites. *J. Mater. Chem.* **2010**, *20*, 1103−1106.
(33) Niu, K. Y.; Yang, J.; Sun, J.; Du, X. W. One-Step Synthesis of MgO Hollow Nanospheres with Blue Emission. *Nanotechnology* **2010**, *21*, 295604.
(34) Camacho-Bragado, G. A.; Elechiguerra, J. L.; Yacaman, M. J. Characterization of Low Dimensional Molybdenum Sulfide Nanostructures. *Mater. Charact.* **2008**, *59*, 204−212.
(35) Frey, G. L.; Tenne, R.; Matthews, M. J.; Dresselhaus, M. S.; Dresselhaus, G. Raman and Resonance Raman Investigation of MoS_2 Nanoparticles. *Phys. Rev. B* **1999**, *60*, 2883−2892.
(36) Berhault, G.; Araiza, L. C.; M?ller, A. D.; Mehta, A.; Chianelli, R. R. Modifications of Unpromoted and Cobalt-Promoted MoS_2 during Thermal Treatment by Dimethylsulfide. *Catal. Lett.* **2002**, *78*, 81−90.
(37) Tuxen, A.; Gøbel, H.; Hinnemann, B.; Li, Z.; Knudsen, K. G.; Topsøe, H.; Lauritsen, J. V.; Besenbacher, F. An Atomic-Scale Investigation of Carbon in MoS_2 Hydrotreating Catalysts Sulfided by Organosulfur Compounds. *J. Catal.* **2011**, *281*, 345−351.
(38) Shi, Y.; Zhou, W.; Lu, A.-Y.; Fang, W.; Lee, Y. H.; Hsu, A. L.; Kim, S. M.; Kim, K. K.; Yang, H. Y.; Li, L. J.; Idrobo, J. C.; Kong, J. Van der Waals Epitaxy of MoS_2 Layers Using Graphene As Growth Templates. *Nano Lett.* **2012**, *12*, 2784−2791.
(39) Cai, G. M.; Jian, J. K.; Chen, X. L.; Lei, M.; Wang, W. Y. Regular Hexagonal MoS_2 Microflakes Grown from MoO_3 Precursor. *Appl. Phys. A: Mater. Sci. Process.* **2007**, *89*, 783−788.
(40) Castro-Guerrero, C. F.; Deepak, F. L.; Ponce, A.; Cruz-Reyes, J.; Valle-Granados, M. D.; Fuentes-Moyado, S.; Galván, D. H.; José-Yacamán, M. Structure and Catalytic Properties of Hexagonal Molybdenum Disulfide Nanoplates. *Catal. Sci. Technol.* **2011**, *1*, 1024−1031.
(41) Zink, N.; Therese, H. A.; Pansiot, J.; Yella, A.; Banhart, F.; Tremel, W. In Situ Heating TEM Study of Onion-like WS_2 and MoS_2 Nanostructures Obtained via MOCVD. *Chem. Mater.* **2008**, *20*, 65−71.
(42) Pyatenko, A.; Yamaguchi, M.; Suzuki, M. Laser Photolysis of Silver Colloid Prepared by Citric Acid Reduction Method. *J. Phys. Chem. B* **2005**, *109*, 21608−21611.
(43) Pyatenko, A.; Yamaguchi, M.; Suzuki, M. Synthesis of Spherical Silver Nanoparticles with Controllable Sizes in Aqueous Solutions. *J. Phys. Chem. C* **2007**, *111*, 7910−7917.
(44) Takami, A.; Kurita, H.; Koda, S. Laser-Induced Size Reduction of Noble Metal Particles. *J. Phys. Chem. B* **1999**, *103*, 1226−1232.

DOI: 10.1021/am508750y
ACS Appl. Mater. Interfaces 2015, 7, 1949−1954

(45) Choi, W.; Cho, M. Y.; Konar, A.; Lee, J. H.; Cha, G.-B.; Hong, S. C.; Kim, S.; Kim, J.; Jena, D.; Joo, J.; Kim, S. High-Detectivity Multilayer MoS_2 Phototransistors with Spectral Response from Ultraviolet to Infrared. *Adv. Mater.* **2012**, *24*, 5832−5836.
(46) Weng, B.; Qiu, J.; Zhao, L.; Chang, C.; Shi, Z. CdS/PbSe Heterojunction for High Temperature Mid-Infrared Photovoltaic Detector Applications. *Appl. Phys. Lett.* **2014**, *104*, 121111.
(47) Itkis, M. E. Bolometric Infrared Photoresponse of Suspended Single-Walled Carbon Nanotube Films. *Science* **2006**, *312*, 413−416.
(48) Tao, T.; Geng, J.; Hong, L.; Huang, W.; Tanaka, H.; Tanaka, D.; Ogawa, T. Temperature-Dependent Current-Voltage and Photoresponsive Properties for Semiconducting Nanodevices Fabricated from an Oligothiazole Dithiol and Gold Nanoparticles. *J. Phys. Chem. C* **2013**, *117*, 25325−25333.
(49) Late, D. J.; Shaikh, P. A.; Khare, R.; Kashid, R. V.; Chaudhary, M.; More, M. A.; Ogale, S. B. Pulsed Laser-Deposited MoS_2 Thin Films on W and Si: Field Emission and Photoresponse Studies. *ACS Appl. Mater. Interfaces* **2014**, *6*, 15881−15888.
(50) Lopez-Sanchez, O.; Lembke, D.; Kayci, M.; Radenovic, A.; Kis, A. Ultrasensitive Photodetectors Based on Monolayer MoS_2. *Nature Nanotechnol.* **2013**, *8*, 497−501.
(51) Li, H.; Wu, J.; Yin, Z.; Zhang, H. Preparation and Applications of Mechanically Exfoliated Single-Layer and Multilayer MoS_2 and WSe_2 Nanosheets. *Acc. Chem. Res.* **2014**, *47*, 1067−1075.

DOI: 10.1021/am508750y
ACS Appl. Mater. Interfaces 2015, 7, 1949−1954